Mineralogical characterization of natural clays from Brazilian Southeast region for industrial applications

(Caracterização mineralógica de argilas naturais provenientes do Sudeste brasileiro visando aplicações industriais)

N. I. Alvarez Acevedo[1], M. C. G. Rocha[1], L. C. Bertolino[2]
[1]Instituto Politécnico, UERJ, R. Bonfim 25, Nova Friburgo, RJ, Brasil 28625-570
[2]Centro de Tecnologia Mineral, Av. Pedro Calmon 900, Rio de Janeiro, RJ, Brasil 21941-908
nacevedo@iprj.uerj.br, mrocha@iprj.uerj.br, lcbertolino@cetem.gov.br

Abstract

Characterization studies of clays are often performed to identify possible markets for these materials. Bearing this in mind, two samples of natural clays from the Southeast region of Brazil were studied. Conventional techniques of characterization were used. Granulometric analysis and determination of cationic exchange capacity of these clays were also performed. Nitrogen adsorption-desorption measurements were used to determine the Brunauer-Emmett-Teller specific surface area, and Barrett-Joyner-Halenda and t-plot pore size analysis were carried out. The results obtained were similar for the two clays. Both present high clay fraction (above 80 wt%) composed of illite, kaolinite and quartz minerals. Stratified illite-smectite structures were also observed. Traces of calcite were detected in one of the clay samples, while traces of montmorillonite were observed in the other sample. These results were corroborated by the low cationic exchange capacity values obtained for both clays. These clays showed good adsorptive properties, evidenced by their specific surface areas, with predominantly mesoporous structures and slit-like pores. According to their features, these clays have potential use as adsorbents to replace more expensive materials due to their easy availability and low cost.
Keywords: characterization techniques, clay minerals, natural clays.

Resumo

Estudos de caracterização de argilas são comumente realizadas para identificar possíveis mercados para esses materiais. Com esse objetivo duas amostras de argilas naturais provenientes do Sudeste brasileiro foram estudadas. Técnicas de caracterização convencionais foram utilizadas. Análise granulométrica e determinação da capacidade de troca catiônica foram também efetuadas. Medições de adsorção/dessorção de nitrogênio foram utilizadas, tanto para obter os valores de área superficial específica das amostras, de acordo com o método de Brunauer, Emmet e Teller, tanto como para a análise do tamanho de poros, usando os métodos de Barret-Joyner-Halenda e t-plot. Os resultados obtidos indicaram que as argilas apresentaram propriedades similares. As duas amostras apresentaram alto conteúdo de fração argila (acima de 80% em massa) composta basicamente dos minerais ilita, caulinita e quartzo. Estruturas estratificadas ilita-esmectita também foram observadas. Uma das amostras apresentou traços de calcita, enquanto a outra apresentou traços de montmorilonita. Os valores baixos de capacidade de troca catiônica obtidos corroboraram estes resultados. As argilas apresentaram boas propriedades adsortivas, evidenciadas pelos valores das suas áreas superficiais específicas, e estruturas predominantemente mesoporosas, constituídas principalmente por poros do tipo fenda. De acordo com estas características, aliadas ao baixo custo e à maior disponibilidade, as argilas estudadas apresentam potencial de utilização como adsorventes, podendo substituir matérias comumente usadas nesse mercado e de maior custo.
***Palavras-chave**: técnicas de caracterização, argilominerais, argilas naturais.*

INTRODUCTION

Clay and clay minerals are abundant, inexpensive and environmentally friendly raw materials. These materials have been familiar to human since the earliest days of civilization [1, 2]. Their wide range of applications includes production of many consumer goods as well as therapeutic systems, often after purification and/or chemical surface modification [3-5]. Clays are defined as materials composed essentially of extremely small particles, composed of one or more members of a group of substances called clay minerals [6]. They also contain other minerals such as carbonates, feldspar, quartz, and (hydr)oxides of iron and aluminum. These components are referred to as associated minerals. Clays also can contain organic matter and other X-ray amorphous materials, which are named associated phases [7]. Clay minerals are composed essentially of silica, alumina or magnesia, or both, and water. Iron, alkalis and alkaline-earth elements are also frequently present in substantial concentrations [6, 8]. In general, clays are very heterogeneous materials whose characteristics depend on their geological formation as well as the extraction location. As a result, a clay deposit

may contain many types of clay minerals slightly different. Therefore, small variations in the content of a particular component can cause drastic changes in the clay properties. Thus, characterization studies are needed to obtain a better knowledge of the industrial potential of a clay deposit, to optimize the extraction and processing of clay materials and to find new areas of applications [9, 10].

Brazil has a large number of clay deposits, but the products obtained are generally of low added value. According to the Ministry of Mines and Energy (MME) [11], the country's confirmed reserves amount to over six billion metric tons. São Paulo state accounts for more than 39% of these reserves, which include clays from four groups: common clays, ball clays, fireclays and bentonite/ Fuller's earth clays. The data presented by the most recent Brazilian Mineral Yearbook, published in 2010, also show that the production of processed clay represents only 14% of the output of raw clays. The consumer market for processed clay is concentrated in three areas: red ceramics (33.53%), civil engineering (21.68%), and floors and coatings (17.71%) [11]. The Taubaté Basin is located along the axis linking the urban centers of São Paulo and Rio de Janeiro, extending along the Paraíba River Valley from Jacareí to the city of Cruzeiro [12]. This region's mineral resources mainly consist of materials for construction (aggregates) and clays [13]. The mineral beds in the central region of this sedimentary basin are composed of interstratified clay minerals (illite-montmorillonite) and smectite, besides of illite, kaolinite and micas, among others [14]. The aim of this study was to characterize two clay samples from the central region of the Taubaté Basin. This is relevant since the results obtained can provide some criteria to develop clay materials with high added value.

MATERIALS AND METHODS

Materials: two clay samples from Taubaté and Tremembé, municipalities of the central region of Taubaté Basin in São Paulo state, Brazil, were used in this study. These samples were identified as Taubaté and Tremembé, according to the location of their respective deposits (Fig. 1). Both clays, with greenish color, were received already disaggregated (granulometry below 74 μm). Each sample was air dried for 24 h. Aliquots of each sample were obtained by homogenization and quartering procedures. One aliquot of each clay sample was fractionated by wet sieving through meshes of 53, 44 and 22 μm, to eliminate impurities such as quartz, feldspar and dolomites, among other non-clay minerals. All fractions obtained were dried at 50 ºC, in a forced-air oven and then weighed. The fraction with grain size less than 22 μm of both clays was disaggregated and homogenized with a mortar and pestle. These fractions were used in the subsequent characterizations.

Characterization methods. *Sedigraph particle size analysis*: was determined using a Micromeritics SediGraph-5100 particle size analyzer. The clay samples for this analysis were prepared by adding 3 g of purified clay in

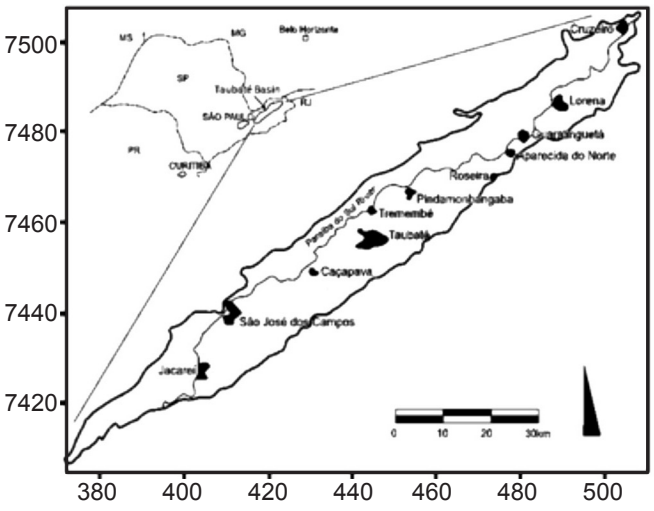

Figure 1: Map showing the locations of the clay deposits. Adapted from [12].
[Figura 1: Mapa geográfico mostrando a localização dos depósitos das argilas em estudo. Adaptado de [12].]

16 mL of deionized water. Then, this dispersion was subjected to magnetic stirring for 13 min and to ultrasonication for 4 min. *Scanning electron microscopy (SEM)/energy dispersive X-ray spectroscopy (EDS)*: to determine the morphology, the clay particles were coated with silver (Bal-Tec/SCD005 sputter coater) under an Ar stream and examined by SEM using a Bruker FEI-Quanta-400 microscope equipped with an Oxford Instruments/Link-ISIS-30 EDS microanalysis system. *X-ray fluorescence (XRF) spectroscopy*: elemental composition of the clay samples was determined using the XRF technique. The analyses were carried out in a Panalytical Axios WDXR fluorescence spectrometer. Loss-on-ignition (LOI) was determined by sample calcination at 1000 ºC for 3 h. *X-ray powder diffraction (XRD)*: mineralogical composition was determined using XRD. Randomly oriented powder samples were used for bulk mineralogy identification. To identify the clay minerals, the clay fraction of each sample was separated by gravimetric sedimentation [15]. Then, oriented powder samples were prepared using the smear-oriented mounting technique [16]. These oriented powder samples were X-rayed under three separate conditions: air-dried (natural), after saturation with ethylene glycol (glycolated), and after heating at 550 ºC for 5 h in a muffle furnace (heated). The XRD patterns were obtained using a Bruker D4 Endeavor diffractometer with CoKα radiation (wavelength of 1.79 Å), 40 kV and 40 mA, in the 2θ range of 4 to 80º, with a scan speed of 0.02º in 2θ/step, and counting time/step of 0.5 s. *Fourier-transform infrared (FTIR) spectroscopy*: FTIR spectra were obtained in a Varian Excalibur 3100 spectrometer, by scanning in the 4000 to 400 cm^{-1} range, with 2 cm^{-1} spectral resolution. Samples for FTIR analysis were prepared using the KBr pressed disk technique. *Thermogravimetric analyses (TGA)*: of clay samples was performed with a PerkinElmer STA-6000 thermal analyzer. The temperature of the samples was increased from 30 to 995 ºC at a heating rate of 10 ºC/min

under air atmosphere. *Methylene blue adsorption tests*: the methylene blue method (ASTM C-837-81 standard) [17] was used to determine the cation exchange capacity (CEC) of the clay samples. The samples were pretreated by drying at 60 ºC for 24 h. Then, they were sieved through a mesh of 74 μm. *Nitrogen adsorption-desorption analysis*: adsorption and desorption isotherms, measured at 77 K, were obtained with a Micromeritics ASAP-2020 accelerated surface area and porosity analyzer. The samples were degassed at 120 ºC for 60 h prior to the measurements at 77 K. Analyses were carried out using the settings and parameter values recommended by the equipment manufacturer [18]. Specific surface areas of the clay samples were determined from multipoint data analysis of adsorption isotherms [18, 19] according to the Brunauer-Emmett-Teller (BET) equation [20]:

$$\frac{1}{v_a(P/Po-1)} = \frac{1}{v_m C_{BET}} + \frac{(C_{BET}-1)}{v_m C_{BET}}\left(\frac{P}{P_O}\right) \qquad (A)$$

where, v_a is the adsorbed volume of nitrogen (N_2) at pressure P, P_o is the saturated vapor pressure of nitrogen at 77 K, v_m is the volume of gas adsorbed to produce an apparent monolayer on the sample surface, and C_{BET} is a dimensionless constant which is related to the enthalpy of adsorption of N_2 on the powder sample. Experimental adsorption data in the relative pressure (P/P_o) range from 0.05 to 0.3 of the isotherms were used to construct the BET graph by plotting $1/[v_a(P/P_o-1)]$ versus P/P_o. The slope (S) and the intercept (Y_{INT}) of the straight line appearing in the BET-plot were used to calculate the specific surface area (S_{BET}) of the clay samples, according to [18, 19]:

$$S_{BET} = \frac{0{,}1620\ nm^2\ X\ (6.023X10^{23})}{(22414\ cm^3_{STP})x(10^{18}\ nm^2/m^2)x(S+Y_{INT})} \qquad (B)$$

In order to verify the applicability of this method, C_{BET} was calculated as $(S/Y_{INT})+1$ [18, 19]. The pore size distribution (PSD) and total pore volume (V_{BJH}) were calculated using the Barrett-Joyner-Halenda (BJH) method [21]. The Halsey thickness equation with Faas correction was used to calculate the thickness (t) of the layer adsorbed on the pore walls, to a given relative pressure [18]. The external surface area (S_{ext}), micropore area (S_{micro}) and micropore volume (V_{micro}) were determined by applying the t-plot method [18]. In this method, the adsorbed layer thickness (t) of N_2 was calculated with the Harkins-Jura equation. A t-curve was then obtained by plotting v_a (Eq. A) versus t [18]. A straight line was obtained by linear fitting of the points in this plot. The intercept of this line with the vertical axis was S_{micro} and the slope was V_{micro}; S_{ext} was determined as $S_{ext}=S_{BET}-S_{micro}$.

RESULTS AND DISCUSSION

The particle size and the mineralogical composition of clays are directly related; clay materials present a higher content of clay minerals in the finer fractions and higher content of non-clay minerals in the coarser fractions [22]. Non-clay minerals are regarded as impurities for many applications, such as nanofillers for polymer composites [23, 24]. Therefore, a fractionation step was necessary to obtain a clay sample with a higher grade of purity. Table I shows that the fraction with average particle size smaller than 22 μm was the major constituent of both clays (94.75 and 82.75 wt%). The features of these fractions evidenced by different characterization techniques are described below.

Granulometric distribution of the clay samples: clay minerals are normally present in the clay fraction of clay materials. These minerals of secondary origin are primarily responsible for the plasticity of a clay-water system [22, 25, 26], among other properties. Fig. 2 presents the granulometric distribution curves of the clay samples. These curves show high concentrations (87.6 and 88.7%) of clay-size particles. Therefore, these clays should present high plasticity and high specific surface area [9, 27]. High values of these properties are important for applications in red ceramics [9, 26, 27].

SEM micrographs and EDS spectra of the clay samples: Figs. 3a and 3b show the SEM micrographs of the clay samples, revealing agglomerates of different sizes with irregular shapes. The presence of agglomerates is characteristic of materials with very fine grain size. Peak intensities of the EDS spectra (Figs. 3c and 3d) revealed that silicon (Si) and aluminum (Al) were the main elements. Iron (Fe), potassium (K), calcium (Ca), magnesium (Mg) and oxygen (O) were other identified elements. All these elements are commonly found in the clay minerals. The presence of silver (Ag) is associated to the metallization of the clay samples for SEM analysis.

Chemical composition by X-ray fluorescence analysis: XRF analysis allows the identification of the chemical constituents and the composition of the minerals contained in clays. According to the XRF analysis (Table II), the chemical composition of both clays was similar. These results are in agreement with the expected chemical composition of the clays, which showed that silica (SiO_2)

Table I - Results of particle size analysis of clay samples (as received).
[Tabela I - Resultados da análise granulométrica das amostras de argilas (como recebidas).]

Clay sample	Particle size fraction retained (wt%)			
	>53 μm	44-53 μm	22-44 μm	<22 μm
Taubaté	3.69	0.02	1.54	94.75
Tremembé	14.29	0.20	2.76	82.75

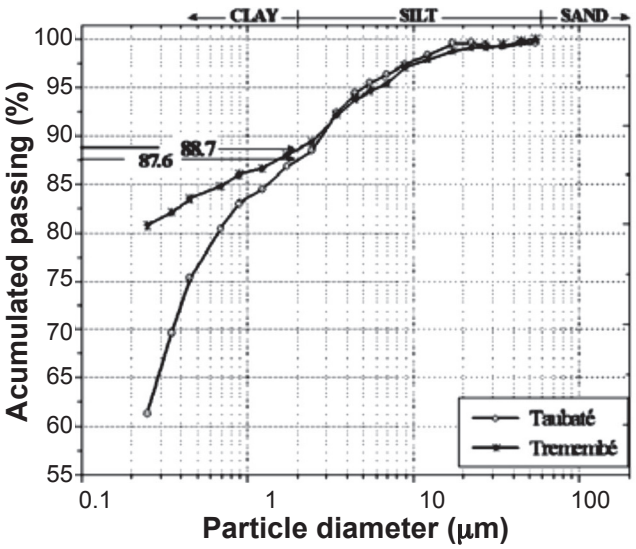

Figure 2: Particle size distribution curves of clay samples (<22 μm fraction).
[Figura 2: Curvas de distribuição granulométrica das amostras de argilas (fração <22 μm).]

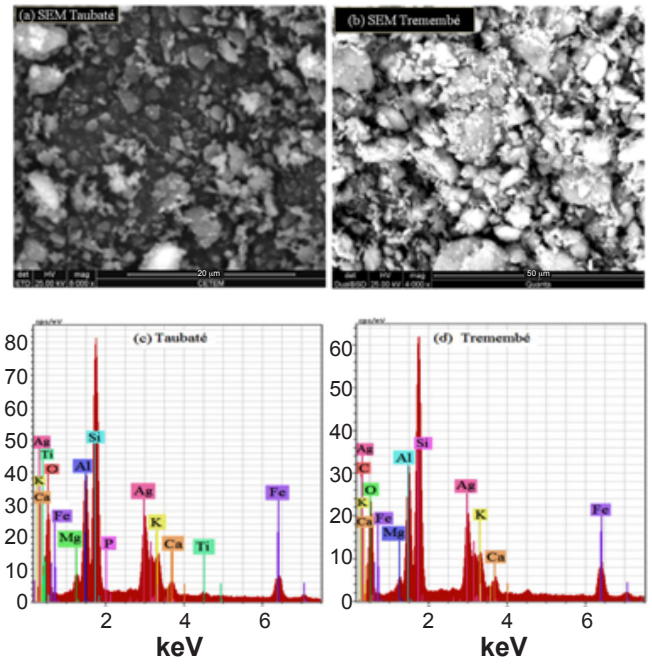

Figure 3: Scanning electron micrographs (a, b), and EDS spectrum of clay samples (c, d).
[Figure 3: Micrografias obtidas por microscopia eletrônica de varredura (a, b) e espectros de EDS das argilas (c, d).]

and alumina (Al_2O_3) are the two main components [28, 29]. These oxides accounted for around 71% of the total mass of the analyzed samples. The silica content indicated the presence of clay minerals, quartz and feldspar, whereas the alumina content indicated kaolinite [27, 28-33]. The molar ratio (SiO_2/Al_2O_3) was 2.76 for the Taubaté sample and 2.57 for the Tremembé sample. The molar ratio value is 1.8 for pure kaolinite [26]. The results obtained suggested the presence of quartz and other silicates in both samples. A published study [34] shows that a molar ratio greater than 2 indicates the presence of montmorillonite. Table II shows that the content of iron oxide (Fe_2O_3) in the Taubaté and Tremembé samples was 7.8% and 9.35%, respectively. These values were in agreement with those reported elsewhere for Brazilian clays, which are generally greater than 4% [9, 10, 31, 32, 34, 35]. Iron could be present in the form of iron ores such as goethite or hematite [31, 34]. Iron and magnesium could be also being present in clay minerals, such as smectites, partially substituting the Al^{3+} cations in the octahedral sites of the clay mineral structure [31, 36]. The presence of calcium oxide (CaO), magnesium oxide (MgO), potassium oxide (K_2O), and sodium oxide (Na_2O) indicated the possible presence of the typical exchange cations in 2:1 clay minerals. Furthermore, the presence of these oxides suggested the presence of mineral contaminants such as dolomite [$CaMg(CO_3)_2$] calcite ($CaCO_3$) and feldspar ($KAlSi_3O_8$-$NaAlSi_3O_8$-$CaAl_2Si_2O_8$) [29, 30]. The total amount of these oxides in the clays under investigation was quite high, around 7.7%. Therefore, both clays may have good flux properties [36, 37]. The high content of Al, Fe and K makes both clays attractive for use in cosmetic applications. These clays contained concentrations of these elements higher than some cosmetic clays characterized by Abel [38]. The content of theses oxides was similar to those of two French clays used for healing [39]. These results suggested that the Taubaté and Tremembé clays can also be used for this application. Among the minor components (less than 1%) contained in both clays, only titanium (Ti) and phosphorus (P) were detected by EDS analysis. As shown by the LOI values (Table II), the Tremembé clay had the highest content of organic matter and volatiles [28].

Both clays presented low CEC values (Table II), 12.7 and 11.3 meq/100 g of dried clay. The smectitic clays present CEC values in the range of 40 to 150 meq/100 g (of dry clay), illite shows CEC values between 10 and 40 meq/100 g, and kaolinite presents CEC values between 3 and 15 meq/100 g [40, 41]. Hence, the CEC values obtained indicated that both clays contained high concentrations of inactive or poorly active materials, such as quartz, kaolinite and illite. The CEC results also showed that the Tremembé clay had higher concentrations of these materials than the Taubaté clay [42]. The CEC values indicate that both clays possibly contained kaolinite or illite or both in high concentrations. The presence of kaolinite and illite combined with a high content of Fe_2O_3 can be useful for developing ultraviolet (UV) protection formulations [43]. Thao [43] showed that kaolins and clays with high content of mica absorb UV-radiation better than bentonites and mixed-layer (illite-smectite) clays, while all of them have equal Fe_2O_3 concentrations.

Mineralogical composition by X-ray diffraction: the XRD patterns of bulk clay samples (data not shown) exhibited intense reflections of kaolinite and quartz. The XRD pattern of Taubaté clay showed the presence of muscovite and traces of calcite, while the XRD pattern of Tremembé clay showed this sample contained illite. The XRD patterns of both clay fractions displayed mainly basal

Table II - Chemical composition, loss on ignition (LOI), in wt%, and cation exchange capacity (CEC), in meq/100 g, of clay samples.
[Tabela II - Composição química, perda por ignição (LOI), em % em massa, e capacidade de troca catiônica (CEC), em meq/100 g, das amostras de argilas.]

Clay sample	SiO_2	Al_2O_3	Fe_2O_3	K_2O	MgO	CaO	TiO_2	P_2O_5	MnO	Na_2O	BaO	SrO	Cr_2O_3	LOI	CEC
Taubaté	50.83	21.48	7.98	3.33	2.78	2.12	0.93	0.50	0.11	0.21	0.05	0.02	0.01	9.62	12.7
Tremembé	49.26	21.32	9.35	2.72	2.61	1.95	0.97	0.45	0.12	0.22	0.05	0.02	0.02	10.91	11.3

reflections of illite, kaolinite and quartz, besides traces of muscovite, phlogopite and biotite. Traces of both calcite and halloysite were present in the Taubaté clay whereas traces of montmorillonite were present in the Tremembé clay. The XRD patterns of oriented natural, glycolated and heated samples (Fig. 4) for the two clay fractions were very similar for all treatments. The diffractograms showed that illite, kaolinite and quartz were the major phases present in the samples. In the XRD patterns of Taubaté clay (Fig. 4a), illite was detected by the peaks (001) at 10.05 Å and (002) at 5.2 Å of illite, and kaolinite was detected by peaks (001) at 7.32 Å and (002) at 3.58 Å. In the XRD patterns of the Tremembé clay (Fig. 4b), illite was identified by the presence of peaks (001) at 10.29 Å and (002) at 4.98 Å while kaolinite was detected by the peaks (001) at 7.16 Å and (002) at 3.58 Å. The illite peak (003) at 3.3 Å was overlapped by the quartz peak at 3.35 Å. Quartz peak (001) was not present [44]. The XRD patterns of glycolated samples showed small

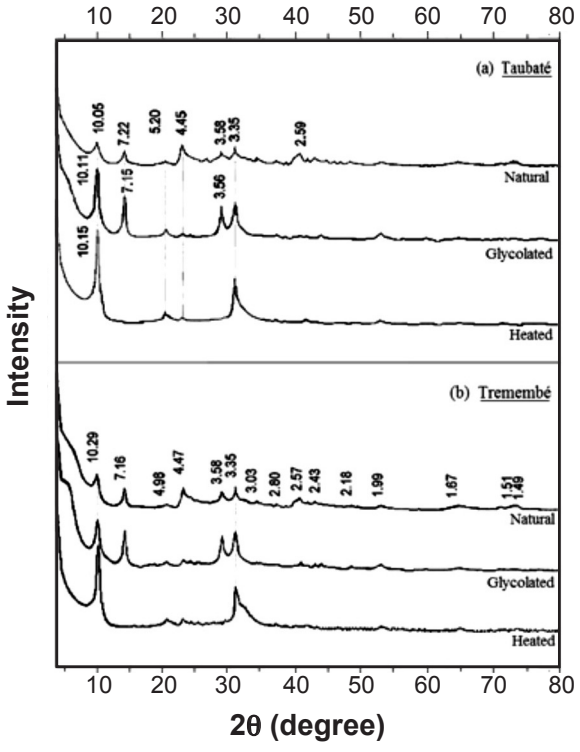

Figure 4: X-ray diffraction patterns of natural, glycolated and heated oriented samples: (a) Taubaté, and (b) Tremembé.
[Figura 4: Difratogramas de raios X das amostras orientadas natural, glicolada e aquecida: (a) Taubaté e (b) Tremembé.]

variations in the position of the illite peak (001) of Taubaté clay, whereas that peak of Tremembé clay remained at 10.29 Å. Thus, the presence of illite was verified in both clays. The shoulder detected to the left of the first-order peak of illite indicated the presence of an inter-stratified illite/smectite structure [45]. This shoulder was more evident in the diffractograms of Taubaté clay. The XRD patterns of heated samples did not show the characteristic peaks of kaolinite (dioctahedral). This result verified the presence of kaolinite in both clays [44]. The results obtained in this work for both clay samples showed that the dominant clay minerals were illite and kaolinite. Mixtures of kaolinite and illite are the most widely used clay material in the ceramics industry. Illite is one of the main clay phases used in the traditional ceramics industry [46]. Both clays also contained quartz as the principal associated mineral and stratified structures of illite and smectite.

Fourier-transform infrared spectra of clay samples: the FTIR spectra of both clay samples (Fig. 5) showed similar profile in two ranges of frequency, 3400 to 3000 cm^{-1} and 1650 to 400 cm^{-1}. Table III shows the principal bands and the possible assignments. From the FTIR spectra obtained, the following minerals were identified: i) illite - indicated by bands at 3697.5, 3622.3, 3446.8/3444.9, 2361, 1635.6/1637.6, 912.3/914.4 cm^{-1} [47], corroborated by the presence of a shoulder near 830 cm^{-1}, along with a band at 1031.9/1033.8 cm^{-1} [48]; ii) disordered kaolinite - indicated by bands at 3697.5, 692.4/694.4 and 912.3/914.4 cm^{-1} [49-52]; iii) quartz - detected by the following bands: doublets bands at 794.7/796.6 cm^{-1} and 752.2/754.2 cm^{-1}, along with a band at 692.4/694.4 cm^{-1}; additionally, the bands at 534.3/530.4 and 470.6/476.4 cm^{-1} gave support to this result [34, 47, 50]; iv) montmorillonite - the characteristic FTIR absorption band of montmorillonite is located in a range from 3300 to 3500 cm^{-1}, commonly around 3400 cm^{-1} [53]; bands at 3622.3, 3446.8/3444.9, 1635.6/1637.6, 1031.9/1033.8, 794.7/796.6 and 470.6/476.4 cm^{-1} showed the presence of montmorillonite in the clays studied [50]; the absorbance at 3620 cm^{-1} is typical for dioctahedral montmorillonites with a high amount of aluminum in the octahedral site; v) illite-smectite - the absorption band at 794.7/796.6 cm^{-1}, related to the angular deformation of the Fe-OH and Mg-OH bonds, highlighted the presence of illite-bentonite mixtures [54]; vi) calcite - the absorption band at 1435.0/1433.1 cm^{-1}, related to the CO stretching of carbonate, was attributed to calcite [50]. Fig. 5 also shows the presence of organic material indicated by the bands at 2920 and 2860 cm^{-1}. These bands

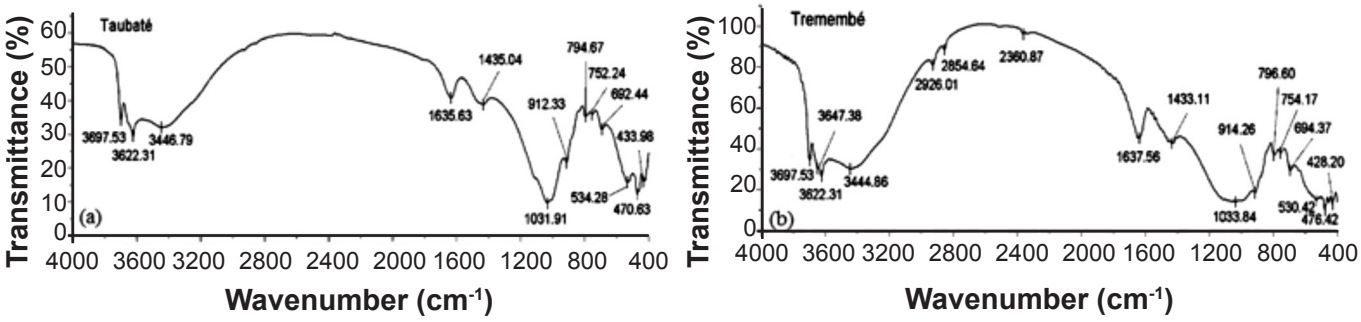

Figure 5: FTIR spectra of Taubaté and Tremembé clays.
[Figura 5: Espectros na região do infravermelho (FTIR) das argilas Taubaté e Tremembé.]

Table III - Main bands (wavenumber in cm^{-1}) identified in FTIR spectra of investigated clays and their possible assignments.
[Tabela III - Principais bandas (número de onda em cm^{-1}) identificadas nos espectros de FTIR das argilas estudadas e suas possíveis atribuições.]

Taubaté	Tremembé	Assignment
3697.53	3697.53	Stretching vibrations of structural hydroxyl of Al-OH group (characteristic absorption band of kaolinite)
3622.31	3622.31	OH stretching of structural hydroxyl groups: Mg-OH/Al-OH/Fe-OH (characteristic absorption band of dioctahedral montmorillonites with a high amount of aluminum)
3446.79	3444.86	H-O-H stretching (axial strain) of hydroxyl groups (absorption band present for almost all clay materials, especially when smectite is the dominant clay mineral)
1635.63	1637.56	Angular deformation of H-O-H molecules of the residual hydration water in the interlayer galleries
1031.91	1033.84	Si-O deformation vibration (absorption band present for all clay minerals)
912.33	914.36	Al-Al-OH deformation (absorption band that confirms the presence of dioctahedral smectite)
794.67	796.60	Si-O stretching (absorption band indicating the presence of quartz)
752.24	754.17	Perpendicular vibration of Si-O (characteristic absorption band of kaolinite)
692.44	694.37	Si-O-Al (octahedral Al) bending vibrations (characteristic absorption band of quartz)
534.28	530.42	Al-O-Si bending vibrations (absorption band observed in all clay minerals' FTIR spectra)
470.63	476.42	Angular deformation of Si-O-Si (absorption band observed in all clay minerals' FTIR spectra)

Table IV - Results of thermogravimetric analysis of the Taubaté and Tremembé clays.
[Tabela IV - Resultados da análise termogravimétrica das argilas Taubaté e Tremembé.]

Clay	30-150 °C		150-400 °C			400-800 °C			Δm total (%)
	T1 (°C)	Δm (%)	T2 (°C)	T3 (°C)	Δm (%)	T4 (°C)	T5 (°C)	Δm (%)	
Taubaté	78.2	6.0	220	~330	1.7	513.2	~700	6.5	14.6
Tremembé	78.2	6.0	250	~350	2.1	510.0	~700	6.0	15.3

were assigned to the vibration of the C-H bond in CH_2 [55]. The greater intensity of bands in the FTIR spectrum of Tremembé clay might be attributed to the higher LOI value of this clay, which was directly related to the organic and volatile materials contained in clays. Smaller peaks at higher frequencies indicated the presence of small amounts of organic material [56]. The results obtained by FTIR were compatible with those obtained by XRD analysis.

Thermogravimetric analysis of clay samples: Table IV gives information about the thermal stability of the clay samples under investigation. Significant mass loss (Δm) occurred in two temperature ranges: i) between 30 and 150 °C, where Δm was 6% for both clays; and ii) between 400 and 800 °C, where Δm was 6.5% for Taubaté clay and 6% for Tremembé clay. TGA showed that the total mass loss was 14.6% for Taubaté clay and 15.3% for Tremembé clay. The mass losses in the temperature range from 30 to 400 ºC were attributed to evaporation of the surface water and the interlayer water. The first endothermic event (dehydration) generally occurs at 100-200 ºC for illite and at 100-250 ºC for

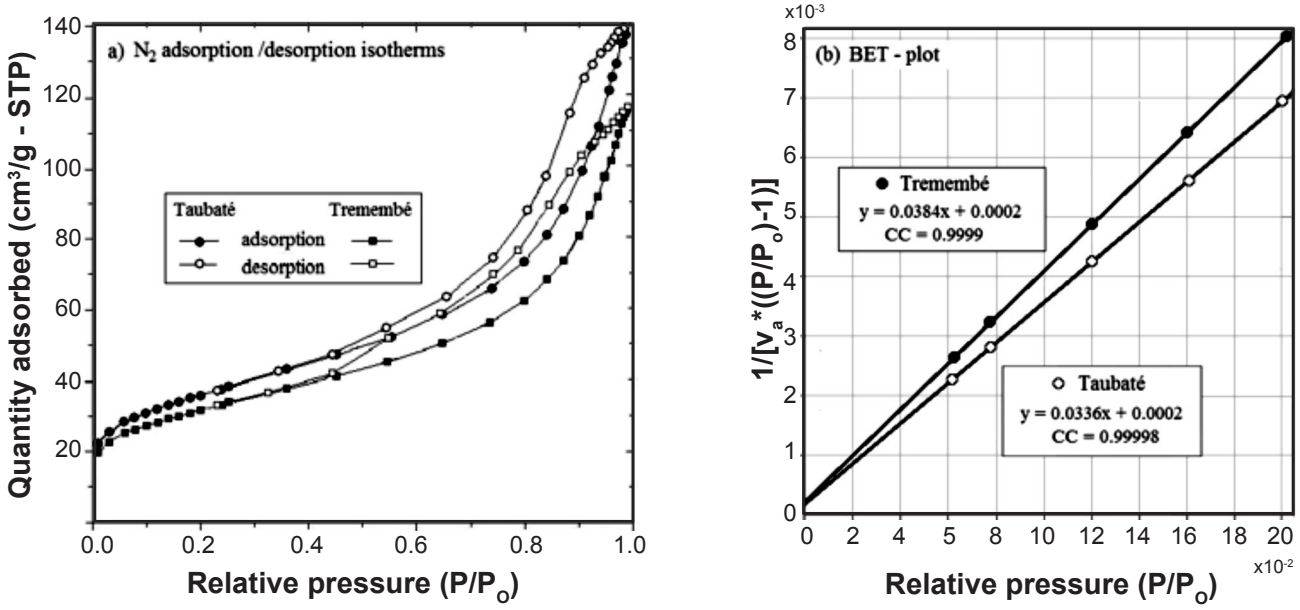

Figure 6: Nitrogen adsorption (closed symbol) and desorption (open symbol) isotherms (a), and BET plot of the investigated clays (b). *[Figura 6: Isotermas de adsorção (símbolo cheio) e dessorção (símbolo vazio) de nitrogênio (a), e gráfico da equação de BET das argilas estudadas (b).]*

Table V - Results of textural analysis of the Taubaté and Tremembé clays.
[Tabela V - Resultados da análise textural das argilas Taubaté e Tremembé.]

Parameter	Taubaté	Tremembé
Correlation coefficient, R	0.999991	0.999983
Specific area, S_{BET} (m^2/g)	128.5±0.3	112.6±0.4
BET constant, C_{BET}	147.07	161.50
External specific area, S_{ext} (m^2/g)	110.51	94.39
Micropore area, S_{micro} (m^2/g)	18.0	18.2
Micropore volume, V_{micro} (cm^3/g)	0.007	0.008
Total pore volume, V_{BJH}* (cm^3/g)	0.2023	0.166
Pore diameter, Dp (Å)	88.56	87.43

* - *volume of pores between 17-300* Å.

smectite [57]. The dehydration temperature of the clays under investigation was T1=78 ºC. Similar T1 values and others lower than T1 have been reported for different Brazilian clays [33, 34]. The temperature peaks T2=220/250 ºC and T3=330/350 ºC indicate the presence of the exchangeable cations, Ca and Mg. These peaks were attributed to the loss of coordinated water molecules of Ca and Mg cations. The presence of Na and K as exchangeable cations was not evidenced in this analysis [10]. T3 can also be attributed to the carbon loss of calcite [58]. A low content of exchangeable cations or high content of kaolinite can be expected in Taubaté clay because T2 was less than 250 ºC [10]. The mass losses at 400-800 ºC occurred by dehydroxylation and formation of quasi-stable dehydroxylated phases. Kaolinite undergoes an endothermic reaction in the 550-600 ºC range, illite in the 500-650 ºC range, and smectite in the 600-700 ºC range [57]. The mass loss of dehydroxylation represents 3.7 and 3.8% of initial mass. The temperature T4=513/510 ºC was associated with the presence of smectites (with a high concentration of iron) or illites or kaolinites, or all them. The transformation from α-quartz to β-quartz occurs at around 565 ºC. The absence of an endothermic peak at this temperature was attributed to a low content of free silica [57-59] in the clays. The temperature T5=700 ºC was associated with: i) dehydroxylation of an aluminous smectite present in a very low concentration; or ii) dehydroxylation of an interstratified smectite; or iii) the structural modification of kaolinite; or all of them. For temperatures above 700 ºC, recrystallization and formation of new phases occur [58]. The results obtained also matched the results of the previous analyses by XRD and FRX.

Nitrogen adsorption-desorption analysis: according to the classification of the International Union of Pure and Applied Chemistry (IUPAC) [60], both clays showed isotherms with profile similar to type IVa isotherms, Fig. 6a. A hysteresis loop and a limit of adsorption in the region of high relative pressure (plateau) are features of these isotherms. The hysteresis loop of isotherms was H3-type, which indicated the presence of slit-shaped pores [60]. Isotherms with this profile have been observed for the adsorption of N_2 and O_2 in montmorillonite clays [61]. The volume adsorbed in the region of very low relative pressures, P/Po below 0.06, indicated some presence of micropores (pores with width below 20 Å [60]). The slope in the region of low relative pressures, 0.06-0.4 range, was attributed to monolayer-multilayer adsorption. The second slope indicated adsorption by capillary condensation. The rapid increment of the amount adsorbed from a relative

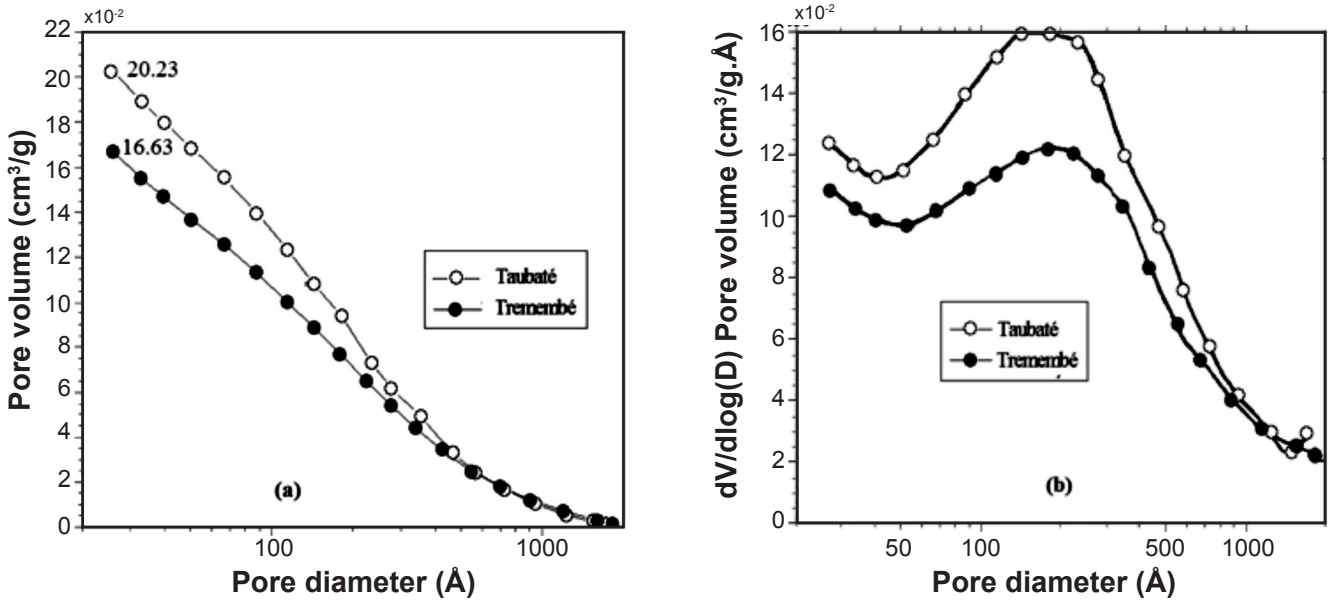

Figure 7: BJH cumulative pore volume (a), and pore size distribution (b) of the investigate clays.
[Figura 7: Volume acumulado de poros (a) e distribuição de tamanho de poros (b) das argilas obtidas pelo método BJH.]

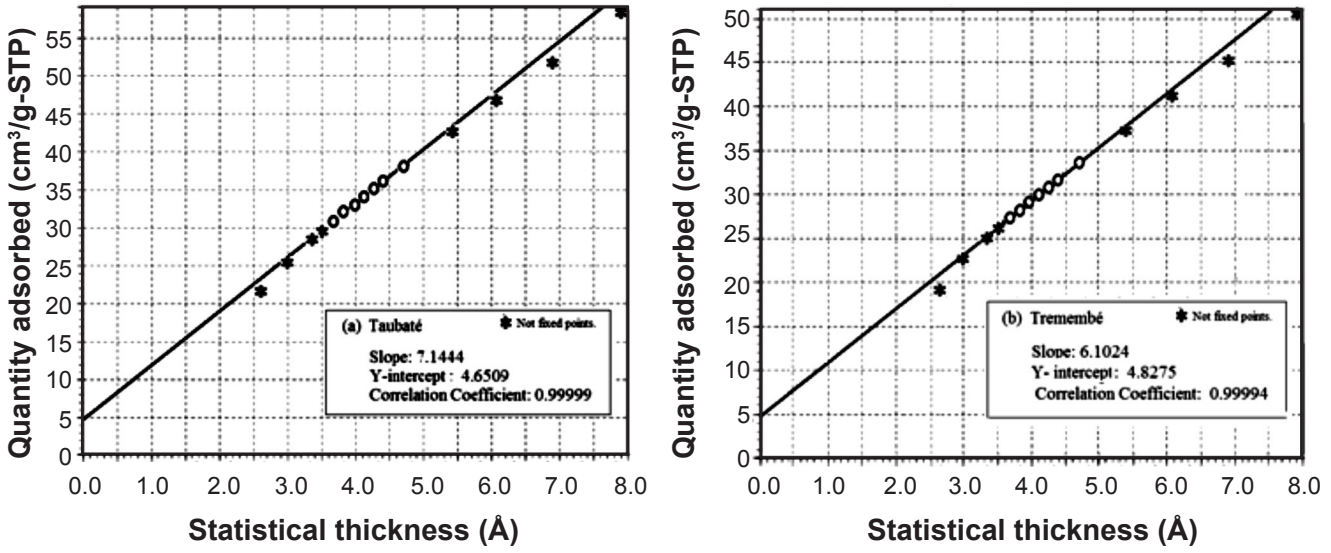

Figure 8: t-curves of the clays: (a) Taubaté, and (b) Tremembé.
[Figura 8: Curva-t -para: (a) argila Taubaté e (b) argila Tremembé.]

pressure close to 0.8 was caused by the filling of the mesopores (pores having width of 20-500 Å [60]) of the largest size as well as those located at the external surface. Considering the adsorbed amounts, a larger surface area was attributed to Taubaté clay. In short, the profile of isotherms and their hysteresis loops indicated that the clays had a porous structure formed mainly by mesopores, associated with some micropores, predominantly with slit-like format. This pore format was consistent with the lamellar structure of clays.

BET specific surface area determination: the BET-plots of each isotherm, Fig. 6b, were linear over the relative pressure range from 0.05 to 0.3. Adsorbed nitrogen quantities smaller or larger than the true values are provided by the BET equation when the relative pressures in the BET-plot are higher or lower than the limits of this linearity range [62]. The correlation coefficient (R, Table V) for both linear BET plots were higher than 0.999 [20]. These results confirmed the appropriateness of using the BET model to determine the specific surface area of the material under investigation. Table V shows the BET specific surface area (S_{BET}) values obtained. These values, 128.5 and 112.6 m^2/g, were higher than those found for some other natural Brazilian clays [63-65]. A "good" smectite clay acid-activated used as a bleaching agent should have a specific surface area in the range of 120-140 $m^2.g^{-1}$ [66]. Thus,

according to this parameter both clays can be classified as good natural adsorbents. The Taubaté clay can be used as a natural bleaching agent. It is important to emphasize that acid treatment can enhance the S_{BET} values of clays [66, 67]. The C_{BET} values obtained, Table V, were within the range from 50 to 300. These results also demonstrated that BET method was suitable to determine the specific surface area of the material [20]. The S_{BET} and C_{BET} values showed an inverse relation. The C_{BET} values indicated that higher microporosity is expected for Tremembé clay, because its larger C_{BET} value [68].

Barrett-Joyner-Halenda (BJH) mesopore analysis: Figs. 7a and 7b show the total pore volume (V_{BJH}) and pore size distribution (PSD) determined by the BHJ method using the adsorption curve data. The use of this curve is recommended considering that it is subject to little influence of the phenomenon referred to as the tensile strength effect [69]. Predominance of mesopores in the size range of 90-400 Å (Fig. 7b) was observed for both clays. This result was in agreement with the observations from isotherm analysis.

t- Plot micropore analysis: the presence of micropores was verified for both clays due to the appearance of positive intercepts in the t-plot (Fig. 8). Table V shows the calculated values of the microporous parameters. These values were low, as expected. The micropore areas (S_{micro}) were much smaller than the external areas (S_{ext}). Furthermore, micropore volumes (V_{micro}) accounted for 4% of the total pore volume. Hence, these results suggested that the external surface was the predominant active surface. These results were typical of a much-closed lamellar structure, preventing access to the interior of the interlamellar space [42].

CONCLUSIONS

The results obtained indicate that the natural clays under investigation were from the same geological formation. Similar results were obtained in the different analyses performed in this work. Both clays present high clay fraction (above 80%) with high concentrations of Fe, K, Ca and Mg oxides. The XRD patterns showed that illite and kaolinite were the dominant clay minerals and that quartz was the main impurity. XRD also showed the presence of interstratified structures in both clays, besides the presence of aluminous smectites in the Tremembé clay. The other characterization techniques gave support to the conclusions described above. The textural characterization indicated that both clays were mesoporous, with a wide distribution of particles sizes and high adsorbent capacity. A possible application for both clays might involve replacement of other more expensive adsorbents, because of these clays' availability, low cost and good adsorption properties.

ACKNOWLEDGMENT

The first author gratefully acknowledges the financial support of CAPES (Coordenação de Aperfeiçoamento de Pessoal de Nível Superior).

REFERENCES

[1] D. Reddy, S.-M. Lee, J.-O. Kim, World Appl. Sci. J. **27**, 11 (2013) 1514.
[2] F. Rocha, P. Suarez, E. Guimarães, Rev. Virtual Quim. **6**, 4 (2014) 1105.
[3] L.B. Williams, S.E. Haydel, Int. Geol. Rev. **52**, 7/8 (2010) 745-770.
[4] E. Iamazaki, M. Paula, Periódico Tche. Química **4**, 8 (2007) 11-21.
[5] M. Reis, "Argilas/lamas portuguesas utilizadas em peloterapia: propriedades físicas e químicas relevantes", Master's thesis, Univ. Aveiro, Portugal (2005).
[6] R. Grim, *Clay mineralogy*, McGraw Hill Book, New York (1968).
[7] F. Bergaya, G. Lagaly, in: F. Bergaya, G. Lagaly (Eds.), *Handbook of clay science*, 2nd Ed., Oxford: Elsevier Sci. (2013) 1.
[8] C. Weaver, L. Pollard, in: *Developments in sedimentology* **15**, Elsevier Sci., New York (1973).
[9] R.S. Macedo, R.R. Menezes, G.A. Neves, H.C. Ferreira, Cerâmica **54**, 332 (2008) 411.
[10] R. Menezes, P. Souto, L. Santana, G. Neves, R. Kiminami, H.C. Ferreira, Cerâmica **55**, 334 (2009) 163.
[11] Min. Minas e Energia, Depto. Nac. Prod. Min., Anuário mineral brasileiro (2010).
[12] A.M.A. Carvalho, A.C. Vidal, C.H. Kiang, Geol. USP, Sér. Cient. **11**, 1 (2011) 19.
[13] T.T. Cruz, "Caracterização de depósitos de areia da bacia sedimentar de Taubaté para a fabricação de vidros", Master's thesis, Univ. S. Paulo (2011).
[14] M. Cabral Jr., J.F.M. Motta, I.S.C. Mello, L.C. Tanno, A. Sintoni, E.D. Salvador, L.A. Chieregatti, Geociências **20**, 1 (2001) 105.
[15] Empr. Brasil. Pesq. Agropec., Manual de preparação de amostras, Centro Nac. Pesq. Solos, Brazil (1997).
[16] M. Jackson, *Soil chemical analysis: advanced course*, Parallel Press, Madison, Wisconsin (1969).
[17] ASTM C837-09, Standard test method for methylene blue index of clay, ASTM Int., West Conshohocken (2014).
[18] Micromeritics, ASAP2020 Operator's manual V4.01 (2011).
[19] Eur. Direct. Quality Medic., in: *European Pharmacopoeia*, 1, cap. 2 (2004) 2811.
[20] S. Brunauer, P.H. Emmett, E. Teller, J. Am. Chem. Soc. **60**, 2 (1938) 309.
[21] E. Barrett, J. Joyner, P. Halenda, J. Am. Chem. Soc. **73**, 1 (1951) 373.
[22] N. Brady, R. Weil, *Elementos da natureza e propriedades dos solos*, Bookman, Porto Alegre, Brazil (2013).
[23] W.S. Cavalcanti, G.F. Brito, P. Agrawal, T.J.A. Mélo, G.A. Neves, M.M. Dantas, Polímeros **24**, 4 (2014) 491.
[24] A.E. Zanini, "Purificação e organofilização de argilas bentonitas para uso em nanocompósitos poliméricos", Master's thesis, Univ. Fed. Campina Grande, Brazil (2008).
[25] J.R. Goes, T.F. Azevedo, T.X.C. Dutra, V.B. Santos, J.B. Severo Jr., L.S. Barreto, Cerâmica **60**, 354 (2014) 211.

[26] C.M.F. Vieira, L.A. Terrones, R. Sánchez, S.N. Monteiro, Cerâmica **53**, 327 (2007) 235.
[27] L. E. Dubois, S. Holgersson, S. Allard, M.E. Malmström, *Water-rock interaction*, P. Birkle, Torres-Alvarado (Eds.), Taylor & Francis, London (2010).
[28] P.S. Santos, *Tecnologia de argilas*, Edgard Blücher, S. Paulo, Brazil (1975).
[29] J.L. Alves, "Estudo e desenvolvimento de uma proposta industrial para selecionar e purificar argilas bentoníticas baseada na lei de Stokes", Master's thesis, Univ. Fed. Bahia, Brazil (2012).
[30] E. Grun, "Caracterização de argilas provenientes de Canelinha/SC e estudo de formulações de massas cerâmicas", Master's thesis, Univ. Est. Santa Catarina, Brazil (2007).
[31] F.A.F. Souto, "Avaliação das características físicas, químicas e mineralógicas da matéria-prima utilizada na indústria de cerâmica vermelha nos municípios de Macapá e Santana-AP", Master's thesis, Univ. Fed. Pará, Brazil (2009).
[32] I.D.S. Pereira, I.A. Silva, J.M. Cartaxo, R.R. Menezes, L.N.L. Santana, G.A. Neves, H.C. Ferreira, Cerâmica **60**, 354 (2014) 223.
[33] I.P. Brito, E.P. Almeida, G.A. Neves, R.R. Menezes, V.J. Silva, L.N.L. Santana, Cerâmica **61**, 360 (2015) 391.
[34] A.M. Morales-Carrera, A.F. Varajão, M.A. Gonçalves, Rev. Esc. Minas **61**, 1 (2008) 97.
[35] M. Cabral Jr., J.F.M. Motta, A.S. Almeida, L.C. Tanno, in: A.B. Luz, F.F. Lins (Eds.), *Rochas e minerais industriais: usos e especificações*, CETEM/MTC, Rio de Janeiro (2005) 583.
[36] C. Gomes, *Argilas: aplicações na indústria*, Ed. Univ. Aveiro, Aveiro (2002).
[37] S. Ferrari, A.F. Gualtieri, Appl. Clay Sci. **32**, 1-2 (2006) 73.
[38] A. Abel, "Caracterização de argilas para uso em saúde e estética", Monography, Univ. Extr. Sul Catarinense, Brazil (2009).
[39] L.B. Williams, S.E. Haydel, R.F. Giese Jr., D.D. Eberl, Clays Clay Miner. **56**, 4 (2008) 437.
[40] I.A. Silva, J.M.R. Costa, R.R. Menezes, H.S. Ferreira, G.A. Neves, H.C. Ferreira, Rev. Esc. Min. **66**, 4 (2013) 485.
[41] L.A. Silva, "Desenvolvimento do processo de obtenção da bentonita organofílica de Moçambique: síntese e caracterização", Master's thesis, Univ. Fed. Santa Catarina, Brazil (2010).
[42] J. Carriazo, R. Molina, S. Moreno, Rev. Colomb. Quím. **36**, 2 (2007) 213.
[43] H.-M. Thao, "Characterization of clays and clay minerals for industrial applications: substitution non-natural additives by clays in UV protection", Doctoral dissertation, Ernst-Moritz-Arndt-Univ. Greifswald, Germany (2006).
[44] A. Scapin, "Aplicação da difração e fluorescência de raios X (WDXRF): ensaios em argilominerais", Master's thesis, Inst. Pesq. Energéticas Nucleares, Brazil (2003).
[45] D.M. Moore, R.C. Reynolds Jr., *X-ray diffraction and the identification of clay minerals*, 2nd Ed., Oxford Univ. Press, New York, USA (1997).
[46] F.O. Aramide, Leonardo J. Sci. **21** (2012) 70.
[47] P.S. Nayak, B.K. Singh, Bull. Mater. Sci. **30**, 3 (2007) 235.
[48] D.C. Nwosu, P.C.N. Ejikeme, M.E. Ebere, IJMSE **4**, 3 (2013) 11.
[49] A.S.P. Paz, R.S. Angélica, R.F. Neves, R. Neumann, G.M. Costa, Cerâmica **57**, 344 (2011) 444.
[50] J. Madejová, Vib. Spectrosc. **31** (2013) 1.
[51] C. Manoharam, P. Sutharsan, S. Dhanapandian, R. Venkatachalapathy, Cerâmica **58**, 347 (2012) 412.
[52] M. Silva, G.P. Silva, P. Santana, Scientia Amazonia **2**, 3 (2013) 54.
[53] A. Kiros, A.V. Gholap, G.E. Gigante, Int. J. Phys. Sci. **8**, 3(2013) 109.
[54] F.Q. Mariani, J.C. Villalba, F.J. Anaissi, Orbital **5**, 4 (2013) 249.
[55] F.J. Jover Maestre (coord.), *La Torreta-El Monastil (Elda, Alicante): del IV al III milenio AC en la cuenca del río Vinalopó*, MARQ, Alicante (2010).
[56] T. Danner, "Reactivity of calcined clays", PhD. Thesis, Norwegian Univ. Sci. Techn., Norway (2013).
[57] R.E. Grim, R.A. Rowland, Am. Min. **27**, 11 (1942) 746.
[58] L. Vaculíková, E. Plevová, Acta Geodyn. Geomater. **2**, 138 (2005) 167.
[59] A.B. Luz, E. Braz, *Quartzo*, CETEM/MCTI, Rio de Janeiro (2000).
[60] M. Thommes, K. Kaneko, A.V. Neimark, J.P. Olivier, F. Rodriguez-Reinoso, J. Rouquerol, K.S.W. Sing, Pure Appl. Chem. **87**, 9-10 (2015) 603.
[61] F. Rouquerol, J. Rouquerol, H. Sing, *Adsorption by powders and porous solids: principles - methodology and applications*, Academic Press London (1999).
[62] M.S.F. Proença, "Preparação de carvões ativados a partir de biomassa e de matrizes zeolíticas", Master's thesis, Univ. Nova Lisboa, Portugal (2011).
[63] D.L. Guerra, C. Airoldi, V.P. Lemos, R.S. Angélica, R.R Viana, Eclet. Quím. **32**, 3 (2007) 51.
[64] D.S. Moraes, R.S. Angélica, C.E.F. Costa, G.N. Rocha Filho, J.R. Zamian, Appl. Clay Sci. **48**, 3 (2010) 475.
[65] C.A.M. Baltar, A.B. Luz, C.H. Oliveira, I.B. Aranha, in: C.A.M. Baltar, A.B. Luz (Eds.), *Insumos minerais para perfuração de poços de petróleo*, CETEM/UFPE, Rio de Janeiro (2003) 15.
[66] A.C.V. Coelho, P.S. Santos, H.S. Santos, Quím. Nova **30**, 5 (2007) 1282.
[67] F.R. Valenzuela-Díaz, P.S. Santos, Quím. Nova **24**, 3 (2001) 345.
[68] R.M.A Cessa, L. Celi, A.C.T. Vitorino, J.O. Novelino, E. Barberis, Rev. Bras. Ci. Solo **33**, 5 (2009) 1153.
[69] J.C. Groen, L.A.A. Peffer, J. Pérez-Ramírez, Microporous Mesoporous Mater. **60** (2003) 1.
(Rec. 28/01/2016, Rev. 20/07/2016, 22/08/2016, 22/09/2016, Ac. 01/11/2016)